Polygenic prediction and gene regulation networks

Juan F Poyatos

Logic of Genomic Systems Laboratory (CNB-CSIC), Madrid, 28049, Spain
jpoyatos@cnb.csic.es

Abstract

Exploring the degree to which phenotypic variation, influenced by intrinsic nonlinear biological mechanisms, can be accurately captured using statistical methods is essential for advancing our comprehension of complex biological systems and predicting their functionality. Here, we examine this issue by combining a computational model of gene regulation networks with a linear additive prediction model, akin to polygenic scores utilized in genetic analyses. Inspired by the variational framework of quantitative genetics, we create a population of individual networks possessing identical topology yet showcasing diversity in regulatory strengths. By discerning which regulatory connections determine the prediction of phenotypes, we contextualize our findings within the framework of core and peripheral causal determinants, as proposed by the omnigenic model of complex traits. We establish connections between our results and concepts such as global sensitivity and local stability in dynamical systems, alongside the notion of sloppy parameters in biological models. Furthermore, we explore the implications of our investigation for the broader discourse surrounding the role of epistatic interactions in the prediction of complex phenotypes.

Introduction

One of the most challenging questions in biology revolves around anticipating phenotypes [1]. From a fundamental perspective, the ability to predict phenotypes, particularly complex ones, sheds light on the coordination among genetic, cellular, and organismal levels [2]. It also elucidates the emergence of robustness and the consequences of its failure, leading to malfunction [3]. With directed application, this knowledge empowers us to intervene more effectively in biology, redirecting disease trajectories, and engineering novel systems with desired properties [4].

However, two complementary research avenues provide seemingly contrasting viewpoints on the accomplishment of this challenge. On one hand, quantitative genetics has successfully developed statistical frameworks that integrate genetic and phenotypic variation to predict phenotypes. These frameworks, which are generally additive, have been effectively applied in agriculture and livestock [5] and also extended into human purposes with the development of polygenic scores (PGSs), which quantify the genetic predisposition of *individuals* to specific traits or diseases [6,7]. This approach signifies progress toward achieving the goal of prediction. On the other hand, molecular genetics is increasingly delineating numerous mechanisms contributing to complex traits. This discipline has emphasized the many nonlinear processes contributing to the phenotype [8]. The presence of nonlinearities at the mechanistic level seems to present a potential limitation to prediction.

These apparent contradictions call for a reassessment of our approach to this problem. One aspect of this revision involves a fundamental discussion on the limitations of variance decomposition in quantitative genetics [9]. This decomposition is not inherently linked to the mechanistic aspects of phenotype generation or gene action [10]. Indeed, the existence of interactions between genes, referred to as biological or functional epistasis, does not necessarily correspond solely to the nonadditive component of variance [11]; it may, in fact, contribute to the additive component [12–15]. Consequently, it is not entirely clear how to reconcile these two aspects.

Moreover, the notion that tools like PGSs would rest on relatively few and strong-effect determinants has been now revised in humans, with the recognition of the abundance of small effect sizes of loci related to complex traits. This is the omnigenic model [16, 17] that defines the genetic determinants of phenotypes in terms of causality, identifying "core" genes with direct effects on the phenotype and "peripheral" genes that influence phenotypes indirectly.

The previous reformulations have underscored the perspective of phenotypes as emergent properties of interacting components within networks, supporting the systemic interpretation of biology advanced in recent years [17–19]. However, arguments regarding the relevance of biological networks in this context are often qualitative and somewhat incomplete. In this work, we aim to provide a formalized examination of this view. We will study the impact of gene regulation on how genetic variation influences phenotypic variation and thus prediction in biology.

To this end, we develop a mathematical framework to emulate the variational approach of quantitative genetics, considering a population of gene regulation networks exhibiting

genetic and phenotypic variation. Genetic variation is displayed in the weights of gene-gene interactions within these networks, which can be interpreted as regulatory interactions [20,21]. Indeed, heritable differences have been shown to be concentrated in regulatory regions in humans [16]. Additionally, phenotypic variation is associated with the diverse steady states observed within these networks.

Using this framework, we calculate a PGS to distinguish the intrinsically nonlinear regulatory connections that most significantly influence the phenotype and to identify any limitations in this prediction. We will investigate how the combination of network architecture and accessible genetic variation influence prediction and its "transferability" [22]. Additionally, this study will aid in delineating core and peripheral causal elements inspired by the omnigenic framework and their relationship with local stability and global sensitivity in dynamical systems. More broadly, our study sheds light on the predominant role of strictly additive models in describing the relationship between genotype and phenotype.

Results

A polygenic score that predicts the phenotype of a regulatory network

We initially examine a population characterized by individual gene regulation networks where nodes represents genes and edges indicate regulatory interaction between them. In this population, the network structure remains constant, but there exists variation in interaction strengths, characterized by deviations around a set of explicit reference values (defining the *reference network*, e.g., Figure 1A, Methods). This strength, or weight, variation can represent mutations in DNA regulatory regions. For each network, we compute the average of the steady-state gene expression associated with a fixed-point attractor reached from a given initial state, which serves as the phenotype. We thus accumulate a dataset comprising genetic variation (changes in weights) and phenotypic variation (changes in average steady-state expression), bringing into line the typical framework of quantitative genetics [9]. We use this data set to derive a multidimensional PGS (Methods) in which regulatory interactions show an additive differential effect size (β) as predictors of the phenotype (Figure 1B).

To better understand the specific connections with stronger effects in the PGS, we utilized both local stability and global sensitivity analysis techniques. On the one hand, considering the linear structure of PGSs, it is reasonable to anticipate that local stability analysis could capture a portion of its signal. This analysis is instrumental in evaluating the system's tendency to deviate linearly from steady-state conditions, aligning with the additive nature of PGSs. The analysis rests on computing the Jacobian matrix of the dynamical equations of the reference network at equilibrium (Strogatz 2018). As anticipated, the product of the Jacobian and the gene steady state, inset in Fig. 1B, reveals interactions determining the phenotype (Figure 1AB, for an exemplary network).

On the other hand, local stability analysis is limited to equilibrium points, disregarding variations across weight parameter space, particularly crucial in nonlinear regulatory networks. Hence, we adopted global sensitivity analysis, decomposing phenotype variance into weight-

specific and collective weight sets' contributions [23]. Specifically, this method yields first-order (S_0^i) and total-order (S_T^i) effect indices for each regulatory connection i, where the former quantifies the main effect contribution of each connection in isolation to the variance of the phenotype, while the latter encompasses both additive and nonadditive effects. From these, we derive the total contribution of nonadditive effects as $\epsilon_T^i = S_T^i - S_0^i$. Notably, strong additive contributions identify connections that play a significant part in the PGS, while strong nonadditive contributions stress weights whose alteration often results in a significant change in the state of the regulated gene, a state flip, inducing a nonlinear effect that percolates throughout the entire network (S1 FigureA). If $S_T^i \sim 0$, then the corresponding regulatory weight can be fixed at any value within its range of uncertainty without appreciably affecting the output variance.

Figure 1C shows an exemplary network in which the sum of first-order effects is approximately 0.72 (what explains the value of R^2 in the PGS), while the sum of the total indices is 1.58; as these two sums are both different from 1, the influence of a single regulation usually depends on the state of others [24]. Indeed, those weights whose $\epsilon_T^i > 0$ indicate such interdependencies, which can often be understood as the state changes (state *flips*) they induce when their values vary, as discussed above.

Complex networks typically result in weaker predictability

To further explore the mechanisms underpinning the accuracy of the statistical prediction, we investigated the dynamical regime of the network. One might hypothesize, for instance, that in the model case of Figure 1A, the network operated within a relatively linear dynamical regime, given the high coefficient of determination of the PGS, $R^2 = 0.69$ (representing the proportion of phenotypic variation explained by the additive PGS). This could be associated with the eigenvalues of the Jacobian matrix; indeed, for this example, all eigenvalues are much smaller than one, indicating that the network readily returns to its original state after experiencing a regulatory quantitative change (Methods). However, the behavior of regulatory networks can transition from fairly linear to strongly nonlinear regimes [25]. Therefore, to systematically examine prediction accuracy, we generated a set of 100 random networks with the same number of nodes and expected connectivity (Methods).

We observed instances of both linear and nonlinear behaviors, as defined with the help of stability analysis (S1 FigureBC). These mechanistic features are partially captured by the statistical indices S_0 (the sum of all individual interactions' additive indexes, S_0^i, equivalent to R^2) and ϵ_T (the sum of all nonadditive indexes, ϵ_T^i), respectively. These parameters determine the location of the network in what we termed the *additive space* (Figure 2).

We then asked whether any structural property ("complexity") would anticipate the network position in this space to note that the presence of two-component positive feedbacks is indeed one such property. Figure 2 shows how the number of these feedbacks (size of points normalized by median value of its population distribution, median value = 2) is enriched in networks with strong nonadditivity (mean number of two-component positive feedbacks for nonadditive networks –with ϵ_T beyond the 80th quartile of its population distribution– is 3.3, expected value with 10000 permutations is 2.47, p-value = 0.005). This makes intuitive

sense as these circuits act as switches of the dynamics in many biological situations [26].

Other measures of network complexity show significant differences, such as path length (how quickly the network reaches equilibrium gene expression; path length is larger the more nonadditive the network is; mean path length for nonadditive networks with ϵ_T beyond the 80th quartile, as before, is 17.9, expected value 15.96, p-value = 0.01), network density (the ratio of the number of edges to the number of possible edges) and clustering coefficient (the probability that adjacent nodes of a given node are connected). Both last scores are also significantly higher for nonadditive networks beyond a given ϵ_T threshold, defined just as previously (S2 Figure).

Genetic variation modulates predictability in a network-dependent manner

However, prediction may be influenced not just by the architecture and (dynamical) action of the network but also by the level of genetic variation within the population [9, 15], so we next evaluated to what extent variation matters. We examined several contrasting scenarios with variation in all weights ranging from 5% (sd = 0.05) of their reference values to as much as 50% (sd =0.5; as compared to the sd=10%, sd = 0.1, used in previous sections). Variation does influence prediction in a way that depends on the specific regulatory network.

Considering the same set of 100 networks, we observed several patterns of dependences that include situations in which there exists a certain variation for maximal or minimal prediction accuracy, respectively (Figure 3A, associated networks shown in S3 Figure). Patterns #1 and #2 typically correspond to networks that respond linearly for low variation, while patterns #3 and #4 work as nonlinear networks for low variation that increase linearity with increased genetic variance, but reaching a maximum (optimal degree of variation) for pattern #3.

This behavior can be understood using again the additive space, but this time we employ it to describe the impact of variation on each network (Figure 3B). We find that pattern #1's phenotypic variation is considerably explained by the additive component S_0 in the range of small genetic variation (weight variation), but that this decreases as genetic variation increases (red to green in Figure 3); the nonadditive ϵ_T part increases what leads to a worsening of prediction accuracy. This is reflected in a diagonal trajectory towards the left in additive space. Other trajectories in this space also clarify the dependence on variation. For instance, the maximum in pattern #3 reflects a trajectory to the right (increased S_0, decreased ϵ_T) that turns back to the regime of high nonadditivity, low additivity as variation intensifies.

Finally, how different is the distribution of additive and nonadditive effects in these scenarios? We computed the correlation of the additive and nonadditive contributions corresponding to each of the genetic variation regimes (S4 Figure). In some cases, the additive determinants change considerably depending on the variation of the population (e.g., #1 in S4 Figure), while in other cases these determinants are relatively stable across conditions (e.g., #2 in S4 Figure). The nonadditivity of determinants typically emerges

(increases) with sd, but could sometimes remain relative stable (e.g., #4 in S4 Figure).

Increased prediction accuracy is associated with the influence of core regulatory interactions

We can reinterpret the previous results in terms of the core/peripheral framework of the omnigenic model [16] by defining *core* interactions as those with the total index contributing beyond 1% ($S_T^i > 0.01$) and the additive component bigger or equal than the nonadditive one ($S_0^i \geq \epsilon_T^i$), *peripheral* interactions as those with $S_T^i > 0.01$ and $S_0^i < \epsilon_T^i$ and *remote* interactions as those with $S_T^i \leq 0.01$. According to this, core and peripheral regulations are causally linked to the phenotype in either an additive or nonadditive manner, respectively, while remote regulations exhibit a very loose connection to the phenotype.

In Figure 4A, it is apparent that as prediction accuracy improves (as indicated by larger R^2 values), the proportion of core (weight) determinants increases, while that of peripheral ones decreases. Additionally, remote weights also exhibit an increase with R^2 values. We also calculated the mean of the absolute effect size, $|\beta|$, associated with each determinant class (Figure 4B). Core determinants predominantly define the PGS beyond an accuracy threshold. In this manner, networks whose associated phenotypes can be predicted by an additive model would only be responsive to perturbations affecting these core connections (see discussioon).

PGSs show imperfect transferability

Finally, we investigated the extent to which a PGS derived under specific conditions could be applicable as a predictive tool in other scenarios. This holds significant implications, particularly concerning the validity of GWAS findings across varied human population [22]. We examine two situations. We first employed a PGS computed with a given variation in the population (10% of variation of each weight around their reference value, i.e., sd = 0.1) corresponding to each of the four patterns (networks) associated with Figure 3 to predict the phenotypes in populations where the available variation is different.

Figure 5A shows the R^2 obtained when applying a PGS computed at sd = 0.1 to populations whose weight distribution correspond to a different variation (values normalized to the R^2 obtained at sd=0.1). We noticed that transferability tends to be effective for conditions comparable to the original training set and that it aligns with the patterns observed in Figure 3. Specifically, a PGS calculated with a population standard deviation (sd) of 0.1 demonstrates increased transferability in situations where it exhibits higher predictability. For instance, there is a noticeable rise in transferability for pattern #2, as depicted in the second row of Fig. 5A, within regimes where the sd is less than 0.1. This trend is consistent with the R^2 values calculated for those corresponding regimes, as shown in Fig. 3A.

In Figure 5B, we modified the network corresponding to pattern #1 (S3 Figure), by changing one weight randomly (Methods). We compute the R^2 using the PGS prediction (PGS computed with the reference network and sd = 0.1) and the phenotype generated with the new mutant network. We also computed a network spectral distance, a measure

of dissimilarity between the reference and the mutant networks (Methods). Perturbations changing considerably the network associated with low transferability. These are perturbations of weights with S_T^i typically large (mean S_T^i for nontransferable mutant graphs = 0.13, mean S_T^i for transferable mutant graphs = 0.01, p-value $< 10^{-4}$).

Discussion

What are the limitations of additive statistical tools in capturing the complexities of genetic influences on complex traits? We approached this question by explicitly incorporating mechanistic gene regulation networks producing phenotypes. By introducing changes to the regulations, we can derive a combination of both genetic and phenotypic variations, allowing us to compute a PGS. In our scenario, the phenotype is directly associated with the steady state of the network.

The network framework is crucial as it offers a rationale for the multitude of determinants identified in GWAS studies [27]. These determinants are often categorized into a handful of core elements, characterized by variations that exert a substantial effect size on the phenotype. Conversely, numerous peripheral elements exhibit weaker effect sizes and are associated with regulatory effects that may not be directly linked to the specific trait under investigation. These are the constituents of the recently introduced omnigenic model [16, 17]; but see also [28].

We demonstrated that local stability analysis partially elucidates the fundamental additive components of the computed PGS. This analytical framework, adept at capturing linear deviations in phenotype, was expected to shed light on determinants of substantial effect size. Furthermore, we employed global sensitivity techniques to quantify both the additive and nonadditive contributions of each regulatory connection to phenotypic variation. Our findings revealed that certain connections exhibit both additive and nonadditive effects on phenotype variation, e.g., Figure 1C, thus reinforcing previous discussions regarding the impact of nonlinear genetic interactions, or biological epistasis, on additive genetic variance [13, 14, 29]. Furthermore, we did observe that the nonlinearity and complexity of the network as a whole, assessed through stability analysis and the use of various metrics such as the presence of two-component positive feedback loops (Figure 2), is correlated with its nonadditivity. Thus, we could partially associate mechanistic and statistical features, a topic of ongoing debate [15]. Networks exhibiting greater linearity tend to yield higher prediction accuracy for the PGS, validating our expectations.

We utilize the sensitivity framework to address three critical topics within this context: the distribution of core, peripheral, and remote determinants, the impact of genetic variation, and the transferability of the prediction. As illustrated in Figure 4, intermediate regimes of predictability exhibit a sparse distribution of core determinants and a multitude of peripheral/remote ones. This pattern closely mirrors what is observed in complex human traits [17]. For instance, the prediction accuracy of height, anatomical features being those with best predictions, is around $R^2 \sim 0.2$ [30]. This would suggest that genomes are in a regime of low (statistical) prediction (Figure 2).

Genetic variation, which encompasses the distribution of alleles within a population, is a component of the genetic architecture underlying a trait [13]. Our findings emphasize its impact on the reliability of predictions and show that this influence is contingent upon the architecture of the network, i.e., the structure of the genotype to phenotype map [29, 31] (Figure 3). In certain scenarios, we observed a degree of stability in the number of determinants (both core and peripheral) across a range of genetic variation in the population (S4 Figure). This observation may offer insights into the similar distribution of selection coefficients recently discussed for some genetic determinants across different traits [32]. If the structure of the gene regulation network leads to a relatively stable set of determinants, and these networks are similar in different traits, then we expect the corresponding prevalence of selection coefficients to be equivalent.

Moreover, it has been discussed that negative selection "flattens" the distribution of heritability [33]. This suggests that selection prevents the clustering of predictors in a few core determinants with significant effects, but rather in a greater number of determinants with smaller effects. We propose here that part of this flattening could also be related to the complexity of the networks, with more nonlinear networks leading to a *de novo* effect size distribution spread along many determinants with small effect (S4 Figure,S5 Figure). Thus, beyond selective constraints, effect sizes and their distribution can also be arranged by network-level factors.

Regarding transferability, our initial findings demonstrate that PGSs exhibit a degree of transferability to populations with relatively similar genetic variation, as one might anticipate (Figure 5A). Furthermore, we investigated how single mutations in the network architecture responsible for generating phenotypic variation could result in prediction failures. Notably, we observed that these mutations predominantly occur in *nonremote* connections ($S_T^i > 0.01$). That phenotypes are only considerable affected by a subset of potential determinants echoes the concept of "sloppy parameters" [34,35]. Indeed, making use of this concept in our context, one could expect that combinations of nonremote weights would lead to "stiff" directions, where small changes result in significant alterations in network behavior and predictions.

Recent studies have also explored the limitations of additive models in capturing the impact of the genetic contribution to phenotypes, employing various mechanistic models that complement our approach. For example, Li et *al.* [1] investigated a deep neural network with varying layers to model the genotype to phenotype mapping. Similar to our findings, they observed that the degree of missing heritability, i.e., the fraction of phenotypic variance explained by genetic variance [9], is proportional to the complexity of the map. In addition, we examined a framework based on genome-scale metabolic reconstructions to address the issue of predictability [36]. These models are more realistic as they encompass all known metabolic reactions and the genes encoding each enzyme for a given organism [37]. Despite the presence of nonadditive effects, we observed that the sum of additive terms accounts for over 75% of the total phenotype variation in this system. This additive component is contingent upon the structure of the metabolic genotype-phenotype map, particularly the monotonic relationship between gene content and phenotype [38, 39]. Moreover, much earlier work, such as that of Frank [40], highlighted how the structure of networks could

delineate a stronger or weaker "zone of nonlinearity", wherein changes in input have roughly linear effects on output. This observation resonates with our results, further corroborating the importance of network structure in delineating the boundaries of linearity in genotype-phenotype mappings.

Overall, our work contributes to evaluating the limitations of using linear models that assume additive genetics. Moreover, it underscores the malleability of gene networks, which can transition their responses from linear to nonlinear functional regimes. It is conceivable that networks operating in a nonlinear regime may undergo *linearization* due to interactions with other networks (via cell-cell interactions) or specific gene-environment interactions, and vice versa, altering the overall prediction accuracy. Exploring how all these nonlinear genetic effects ultimately influence phenotypic variation remains an open avenue for further investigation.

Methods

Gene regulation network model. We consider regulatory reference networks constituted by N genes that regulate each other, where every possible regulation between genes is created with the same constant probability, c ($0 \leq c \leq 1$), according to an Erdös-Rényi model [41] (networks will not contain any self-loops) and stored in a matrix W. Weights on this matrix follow a normal distribution with mean 0 and standard deviation 1. The expression of the genes at a given time t is defined by a gene expression vector $\vec{G}(t) = [g_1(t), \ldots, g_N(t)]$ whose (discrete) time dynamics follows a set of nonlinear coupled difference equations: $g_i(t+1) = f[\sum w_{ij} g_j(t)]$. Here, f is a sigmoidal function $f(x) = 2/[1 + \exp(-ax)] - 1$, with a controlling the steepness of the sigmoid (the larger a, the steeper) that normalizes expression values in the range [-1 (`off` state of a gene), 1(`on` state of a gene)]. This model developed in [20] has its roots in statistical physics [42]. In our simulations, we considered $N = 10, c = 0.3$, and $a = 10$. Studies involving larger networks and alternative connectivities will be the focus of future work.

Network dynamics. We set the initial state $\vec{G}(0)$ as a vector of $g_i(0)$= 1 or -1 randomly assigned with probability 1/2. The states change following the difference equations defined before until it reaches an equilibrium. We selected genetic regulatory networks that lead to a fixed-point equilibrium within a number of 100 iterations [20, 21]. We followed previous protocols to numerically identify when the equilibrium $\vec{G}(\mathrm{t_{eq}})$ is reached. This is recognized when a measure of how much the state is changing for a specified time period is considerably small (ψ score from [21]). The number of iterations to equilibrium is named *path length*.

Genetic and phenotypic variation. We generate genetic variation within a population by sampling gene-gene interaction weights from a normal distribution with mean equal to the specific weight w_{ij}, of the corresponding reference network, and standard deviation given by 10% of that value, unless indicated otherwise. For each member of a population, we maintained the same fixed initial state to compute the steady-state expression, the mean of

which corresponds to the individual network phenotype. We considered a population size of 10^4 individuals.

Network nonlinearity. We quantify the nonlinear dynamical regime of a given reference network by computing the eigenvalues of its Jacobian at equilibrium [43]. We typically find a combination of eigenvalues equal to 0 and less than 1. When a discrete dynamical map as our case presents such combination, it suggests a mixture of stability conditions and dynamic behaviors. Eigenvalues equal to 0 indicate neutral stability, where the system remains at equilibrium without evolving over time. Perturbations around the equilibrium state do not cause the system to diverge or converge but rather stay in the vicinity of the equilibrium point. We computed the number of 0 eigenvalues for each network and showed that is associated with additivity (S1 FigureB, right panel). Moreover, eigenvalues less than 1 indicate stable dynamics, where perturbations around the equilibrium state decay over time, leading the system back towards equilibrium. This implies convergence towards the stable fixed point. We showed that the maximal value of these eigenvalues for each reference network considered in Fig. 2) associated with nonadditivity (S1 FigureB, left panel). Thus, this combination of zero eigenvalues and eigenvalues less than 1 defines a kind of mechanistic information that helps explain the statistical additive space.

Polygenic score. We define the network phenotype, y, as the *mean steady state expression* of its genes and use a high-dimensional regression framework for polygenic modeling and prediction: $\vec{y}_{P\times 1} = \mathrm{G}_{P\times I}\vec{\beta}_{I\times 1} + \vec{\epsilon}_{P\times 1}$, where P is the population size, I is the number of nonzero determinants, y is the vector of phenotypes, G is the genotype matrix, $\vec{\beta}$ is the vector of effect sizes of the genes, and $\vec{\epsilon}$ is some noise assumed normal with unknown variance. The generated data was fitted using the Least Absolute Shrinkage and Selection Operator (`LASSO`), a type of regression that, within Bayesian statistics, assumes prior Laplace distributions for each coefficient rather than uniform distributions, as in the case of Ordinary Least Squares. As a result, with `LASSO`, some parameters are automatically shrunk to zero [44] making it a remarkable alternative to pruning and thresholding (P+T) or other regularization methods [6, 45]. Additionally, we determine the optimal value of the shrinkage parameter using five-fold cross-validation.

Numerical Computation of sensitivity indices. We followed [24]. In brief, we first generate a $(N_{\mathrm{sobol}}, 2k)$ matrix of random numbers (k is the number of regulatory connections) and define two matrices of data (A and B), each containing half of the sample. N_{sobol} was taken to be 5×10^4. We define a matrix C_i formed by all columns of A except the i-th column, which is taken from B. We then compute the model output for all the input values across the sample matrices A, B, and C_i, obtaining three vectors of model outputs of dimension $N_{\mathrm{sobol}} \times 1 : \vec{y}_A = f(A), \vec{y}_B = f(B)$ and $\vec{y}_{Ci} = f(C_i)$. From these vectors we can compute the first- and total-effect indices for a given weight [24]; see also supplement in [36]. The bars in Fig. 1 represent the mean values of these indices, with small standard deviations (not shown for simplicity of presentation).

PGS transferability. To assess transferability, we obtain a PGS in a reference condition and then apply it to predict phenotypes under various conditions, such as different standard deviations or networks. We calculate the corresponding R^2 between the predicted and observed phenotypes as a measure of transferability. The graph spectral distance between two networks serves as a measure of dissimilarity between them. Spectral distance is defined as $d(G_1, G_2) = \sqrt{\sum_{i=1}^{N} (|\lambda_i(G_1)| - |\lambda_i(G_2)|)^2}$, where $|\lambda_1(G|) > |\lambda_2(G)|, \ldots$ are the absolute value of the eigenvalues of each network in decreasing order and N the number of nodes.

Supporting Information

S1 Figure

State flip and network nonlinearity. A) We defined a "state flip" as occurring when a displacement δw from a wild-type weight value w generates a change in the sign of the expression of a given gene i from time t to time $t+1$, i.e., $\text{sign}[g_i(t)] \neq \text{sign}[g_i(t+1)]$. Recall that $g_i(t+1) = f[\sum w_{ij} g_j(t)]$, with f being a sigmoidal function $f(x) = 2/[1+\exp(-ax)] - 1$. This flip is an indication of the nonlinear dynamics. **B)** We assess the nonlinear dynamics of each reference network in Fig. 2 based on the maximal absolute value of the eigenvalues of the Jacobian matrix at equilibrium (left panel) and the count of eigenvalues with a value of zero (right panel). A smaller dot on the left indicates a smaller value of this eigenvalue and thus higher stability of the network. Conversely, a larger dot on the right indicates a larger number of zero eigenvalues and again higher stability (Methods).

S2 Figure

Network nonlinearity and prediction accuracy. A) The ratio of the number of edges to the total number of edges (network density) is significantly bigger in networks with ϵ_T beyond the 80th quartile of the population distribution that are associated to lower prediction accuracy (R^2). **B)** The probability that adjacent nodes of a given node are connected (clustering coefficient) is significantly bigger in nonadditive networks with ϵ_T beyond the 80th quartile. Histograms show the null distribution of either score (10000 randomizations of the assignment of ϵ_T values to the related score) and red vertical dashed line the corresponding observed value. See also Figure 2, main text.

S3 Figure

Network structures. Networks corresponding to patterns #1 to #4, A) to D), respectively, in Figure 3. Associated R^2 at sd= 0.01 are $R^2_A = 0.86, R^2_B = 0.28, R^2_C = 0.54, R^2_D = 0.25$.

S4 Figure

Additive and nonadditive effects and genetic variation. For each pattern in Figure 3 (A-D) (networks shown in Fig. S3) we computed the correlation between the additive, S_0^i or nonadditive, ϵ_T^i, contributions to variance computed for different genetic variation (top

figures on each panel). We also computed how these contributions change for each weight determinant (bottom figures on each panel). This plot highlights the range of stability of the additive/non additive role of each weight on the phenotypic variance. Note that some cases, e.g., #4, show considerable stability.

S5 Figure

Polygenicity, effect size and nonadditivity. Polygenicity quantified as the number of weights with effect size β different from zero tends to decrease with mean effect size and increase with nonadditivity, although the tendency is weak but illustrative. Figures show the values for each of the 100 random network and a linear regression (continuous line) and confidence intervals (filled points); A) $R^2 = 0.046$, B) $R^2 = 0.013$.

Acknowledgments

Thanks to all members and visitors of the LoGS lab for the discussions. This work was supported by grant PID2019-106116RB-I00 from the Spanish Ministry of Economy and Competitiveness with European Regional Development Fund.

References

1. Jingjing Li, Xiao Li, Sai Zhang, and Michael Snyder. Gene-Environment Interaction in the Era of Precision Medicine. *Cell*, 177(1):38–44, March 2019.

2. Eric H. Davidson and Douglas H. Erwin. Gene Regulatory Networks and the Evolution of Animal Body Plans. *Science*, 311(5762):796–800, February 2006.

3. Kamil A. Lipinski, Louise J. Barber, Matthew N. Davies, Matthew Ashenden, Andrea Sottoriva, and Marco Gerlinger. Cancer Evolution and the Limits of Predictability in Precision Cancer Medicine. *Trends in Cancer*, 2(1):49–63, January 2016.

4. Madeline A. Lancaster and Juergen A. Knoblich. Organogenesis in a dish: Modeling development and disease using organoid technologies. *Science*, 345(6194):1247125, July 2014.

5. Cedric Gondro. *Genome-wide association studies and genomic prediction*. Number 1019 in Methods in molecular biology. Humana Press, New York, 2013.

6. Frank Dudbridge. Power and predictive accuracy of polygenic risk scores. *PLoS genetics*, 9(3):e1003348, March 2013.

7. Ali Torkamani, Nathan E. Wineinger, and Eric J. Topol. The personal and clinical utility of polygenic risk scores. *Nature Reviews Genetics*, 19(9):581–590, September 2018.

8. Patrick C. Phillips. Epistasis — the essential role of gene interactions in the structure and evolution of genetic systems. *Nature Reviews Genetics*, 9(11):855–867, November 2008.

9. Douglas S. Falconer and Trudy Mackay. *Introduction to quantitative genetics*. Pearson, Prentice Hall, Harlow, 4. ed., edition, 2009.

10. M. W. Feldman and R. C. Lewontin. The Heritability Hang-Up: The role of variance analysis in human genetics is discussed. *Science*, 190(4220):1163–1168, December 1975.

11. Wen Huang and Trudy F. C. Mackay. The Genetic Architecture of Quantitative Traits Cannot Be Inferred from Variance Component Analysis. *PLOS Genetics*, 12(11):e1006421, November 2016.

12. William G. Hill, Michael E. Goddard, and Peter M. Visscher. Data and Theory Point to Mainly Additive Genetic Variance for Complex Traits. *PLoS Genetics*, 4(2):e1000008, February 2008.

13. Trudy F. C. Mackay. Epistasis and quantitative traits: using model organisms to study gene–gene interactions. *Nature Reviews Genetics*, 15(1):22–33, January 2014.

14. Thomas F. Hansen. Measuring Gene Interactions. In Jason H. Moore and Scott M. Williams, editors, *Epistasis*, volume 1253, pages 115–143. Springer New York, New York, NY, 2015. Series Title: Methods in Molecular Biology.

15. Richard F. Campbell, Patrick T. McGrath, and Annalise B. Paaby. Analysis of Epistasis in Natural Traits Using Model Organisms. *Trends in Genetics*, 34(11):883–898, November 2018.

16. Evan A. Boyle, Yang I. Li, and Jonathan K. Pritchard. An Expanded View of Complex Traits: From Polygenic to Omnigenic. *Cell*, 169(7):1177–1186, June 2017.

17. Xuanyao Liu, Yang I. Li, and Jonathan K. Pritchard. Trans Effects on Gene Expression Can Drive Omnigenic Inheritance. *Cell*, 177(4):1022–1034.e6, May 2019.

18. Nasa Sinnott-Armstrong, Sahin Naqvi, Manuel Rivas, and Jonathan K Pritchard. GWAS of three molecular traits highlights core genes and pathways alongside a highly polygenic background. *eLife*, 10:e58615, February 2021.

19. Iain Mathieson. The omnigenic model and polygenic prediction of complex traits. *The American Journal of Human Genetics*, 108(9):1558–1563, September 2021.

20. Andreas Wagner. Does Evolutionary Plasticity Evolve? *Evolution*, 50(3):1008–1023, June 1996.

21. M. L. Siegal and A. Bergman. Waddington's canalization revisited: Developmental stability and evolution. *Proceedings of the National Academy of Sciences*, 99(16):10528–10532, August 2002.

22. Ying Wang, Jing Guo, Guiyan Ni, Jian Yang, Peter M. Visscher, and Loic Yengo. Theoretical and empirical quantification of the accuracy of polygenic scores in ancestry divergent populations. *Nature Communications*, 11(1):3865, July 2020.

23. I.M Sobol. Global sensitivity indices for nonlinear mathematical models and their Monte Carlo estimates. *Mathematics and Computers in Simulation*, 55(1-3):271–280, February 2001.

24. Andrea Saltelli. *Global sensitivity analysis: the primer*. Wiley, Chichester, West Sussex, 2008.

25. Uri Alon. *An introduction to systems biology: design principles of biological circuits*. CRC Press, Taylor & Francis Group, Boca Raton London New York, second edition edition, 2019.

26. Raúl Guantes and Juan F. Poyatos. Multistable Decision Switches for Flexible Control of Epigenetic Differentiation. *PLoS Computational Biology*, 4(11):e1000235, November 2008.

27. Peter M. Visscher, Naomi R. Wray, Qian Zhang, Pamela Sklar, Mark I. McCarthy, Matthew A. Brown, and Jian Yang. 10 Years of GWAS Discovery: Biology, Function, and Translation. *The American Journal of Human Genetics*, 101(1):5–22, July 2017.

28. Naomi R. Wray, Cisca Wijmenga, Patrick F. Sullivan, Jian Yang, and Peter M. Visscher. Common Disease Is More Complex Than Implied by the Core Gene Omnigenic Model. *Cell*, 173(7):1573–1580, June 2018.

29. Richard C. Lewontin. *The genetic basis of evolutionary change*. Number 25 in Columbia biological series. Columbia Univ. Pr, New York, 1974.

30. Buu Truong, Leland E. Hull, Yunfeng Ruan, Qin Qin Huang, Whitney Hornsby, Hilary Martin, David A. Van Heel, Ying Wang, Alicia R. Martin, S. Hong Lee, and Pradeep Natarajan. Integrative polygenic risk score improves the prediction accuracy of complex traits and diseases. *Cell Genomics*, page 100523, March 2024.

31. P. Alberch. From genes to phenotype: dynamical systems and evolvability. *Genetica*, 84(1):5–11, May 1991.

32. Yuval B. Simons, Hakhamanesh Mostafavi, Courtney J. Smith, Jonathan K. Pritchard, and Guy Sella. Simple scaling laws control the genetic architectures of human complex traits. *BioRxiv*, 10.1101/2022.10.04.509926, October 2022.

33. Luke J. O'Connor, Armin P. Schoech, Farhad Hormozdiari, Steven Gazal, Nick Patterson, and Alkes L. Price. Extreme Polygenicity of Complex Traits Is Explained by Negative Selection. *The American Journal of Human Genetics*, 105(3):456–476, September 2019.

34. K S Brown, C C Hill, G A Calero, C R Myers, K H Lee, J P Sethna, and R A Cerione. The statistical mechanics of complex signaling networks: nerve growth factor signaling. *Physical Biology*, 1(3):184–195, October 2004.

35. Ryan N Gutenkunst, Joshua J Waterfall, Fergal P Casey, Kevin S Brown, Christopher R Myers, and James P Sethna. Universally Sloppy Parameter Sensitivities in Systems Biology Models. *PLoS Computational Biology*, 3(10):e189, October 2007.

36. Pablo Yubero, Alvar A. Lavin, and Juan F. Poyatos. The limitations of phenotype prediction in metabolism. *PLOS Computational Biology*, 19(11):e1011631, November 2023.

37. Bernhard Palsson. *Systems biology: properties of reconstructed networks*. Cambridge University Press, Cambridge ; New York, 2006. OCLC: ocm62421240.

38. Daniel M Weinreich. The Rank Ordering of Genotypic Fitness Values Predicts Genetic Constraint on Natural Selection on Landscapes Lacking Sign Epistasis. *Genetics*, 171(3):1397–1405, November 2005.

39. A. B. Gjuvsland, J. O. Vik, J. A. Woolliams, and S. W. Omholt. Order-preserving principles underlying genotype-phenotype maps ensure high additive proportions of genetic variance. *Journal of Evolutionary Biology*, 24(10):2269–2279, October 2011.

40. Steven A. Frank. Population and Quantitative Genetics of Regulatory Networks. *Journal of Theoretical Biology*, 197(3):281–294, April 1999.

41. Béla Bollobás. *Random graphs*. Number 73 in Cambridge studies in advanced mathematics. Cambridge Univ. Press, Cambridge, 2. ed., edition, 2008.

42. Janna L. Fierst and Patrick C. Phillips. Modeling the evolution of complex genetic systems: The gene network family tree. *Journal of Experimental Zoology Part B: Molecular and Developmental Evolution*, 324(1):1–12, January 2015.

43. Steven H. Strogatz. *Nonlinear Dynamics and Chaos*. CRC Press, 0 edition, May 2018.

44. Bradley Efron and Trevor Hastie. *Computer age statistical inference: algorithms, evidence, and data science*. Number 6 in Institute of Mathematical Statistics monographs. Cambridge University Press, Cambridge, United Kingdom, student edition edition, 2021.

45. Naomi R. Wray, Jian Yang, Ben J. Hayes, Alkes L. Price, Michael E. Goddard, and Peter M. Visscher. Pitfalls of predicting complex traits from SNPs. *Nature Reviews. Genetics*, 14(7):507–515, July 2013.

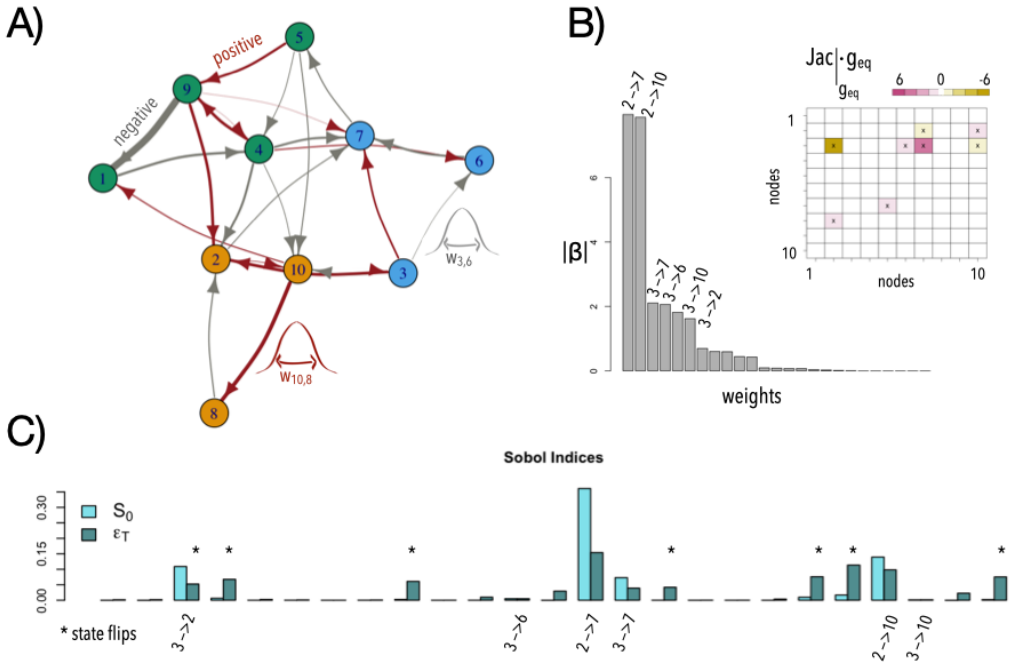

Figure 1. PGS, local stability and global sensitivity analysis of a model network. **A)** Example of a reference network with $N = 10$ genes. We develop a variational framework in which each network in the population exhibits the same structure, but its weights are sampled from normal distributions centered around the weights of the reference network, with variations around 10% of these values (sd = 0.1, two examples are shown). Red and gray edges represent positive and negative interactions, respectively. Nodes are colored here following a simulated annealing procedure to identify communities in a network. **B)** Absolute value of effect size, $|\beta|$, for each regulatory connection in the PGS obtained. Top values are associated to their respective edges. Inset. The product of the Jacobian matrix at equilibrium and the steady-state gene expression of the reference network predicts the weights of the top strength in the PGS. Color highlights the strength of the values. **C)** Sobol indices where S_0^i describe the additive contribution and ϵ_T^i the nonadditive contribution of each edge i to the variation of the phenotype. Asterisks indicate those weights that contribute to state flips when subjected to variation (see main text). Here $i \to j$ represents the regulation of i on j with weight $w_{i,j}$. Time to reach equilibrium ("path length") of model network = 18 (time steps), PGS $R^2 = 0.69$.

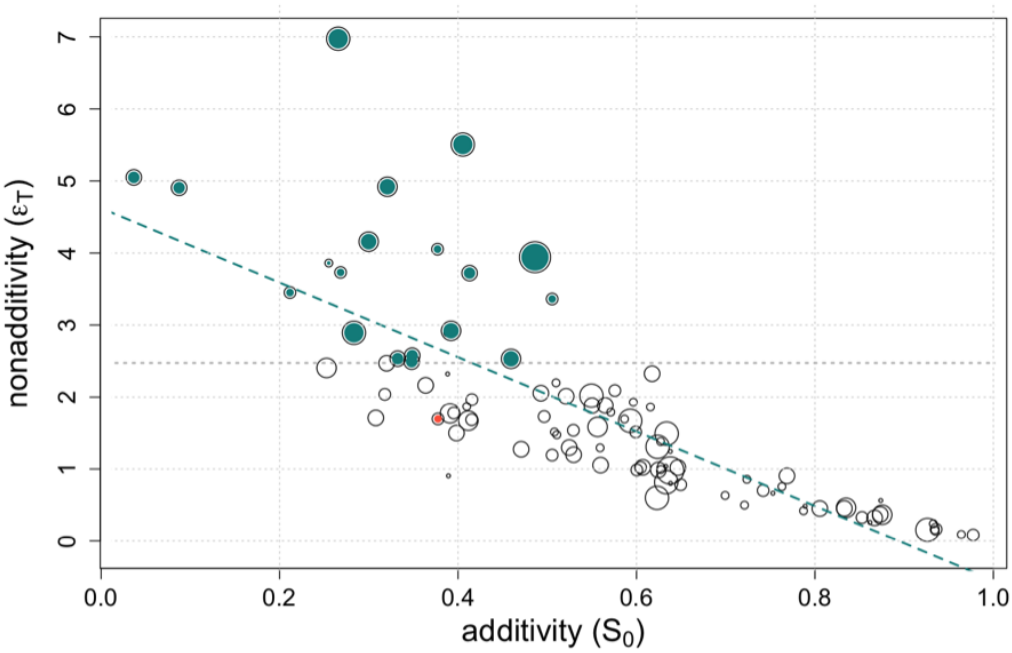

Figure 2. The additivity space of gene regulation networks and the presence of two-component positive feedbacks. We computed the sum of Sobol's additive (S_0) and nonadditive (ϵ_T) indexes for each network across a dataset consisting of 100 random networks. Dot size represents the number of two-component positive feedbacks found on each network normalized by the median value of the entire population (median = 2). Networks with nonadditivity values beyond the 80th quartile of the population (indicated by the dashed gray line, networks highlighted in green) are enriched in two-component positive feedbacks (observed mean number = 3.3, expected mean number = 2.47, p-value = 0.005 after 10000 permutations). The red dot denotes a network with two two-component positive feedbacks, while the green dashed line illustrates the additive-nonadditive effects trade-off.

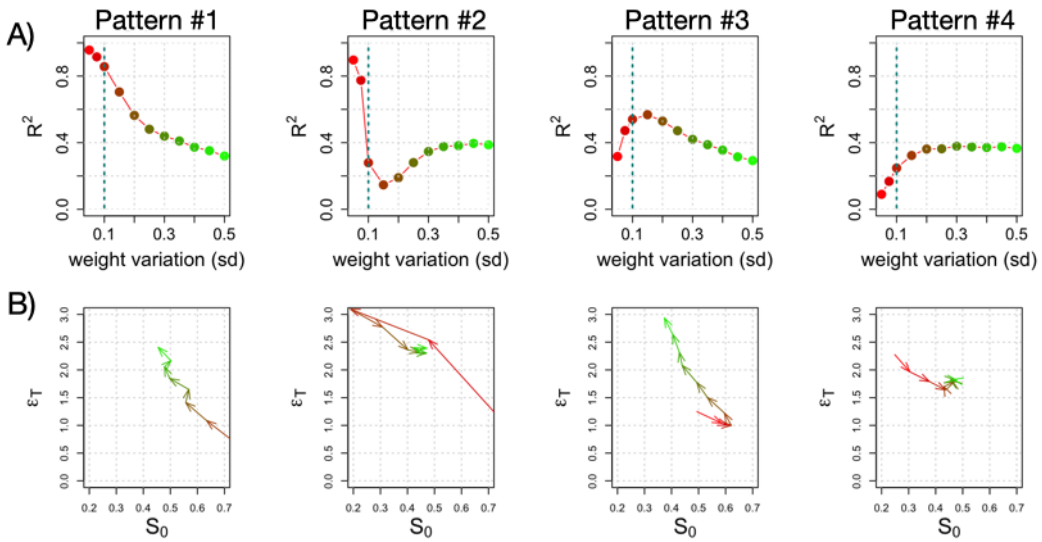

Figure 3. Genetic variation and its influence on prediction. A) We show four patterns of how PGS prediction accuracy (in terms of R^2) changes as the genetic variation (sd of weights in the population) changes. The case of sd = 0.1 is indicated by dotted line. Patterns #1, #2 show strong prediction with small variation. Patterns #3, #4 show weak prediction with small variation that increases with more variation (#3 exhibits an optimal genetic variation for prediction). **B)** Trajectory of the patterns above in the additive space (S_0, ϵ_T). Red to green colors indicate a transition from lower to higher variation of the weights of the regulatory connections in the population.

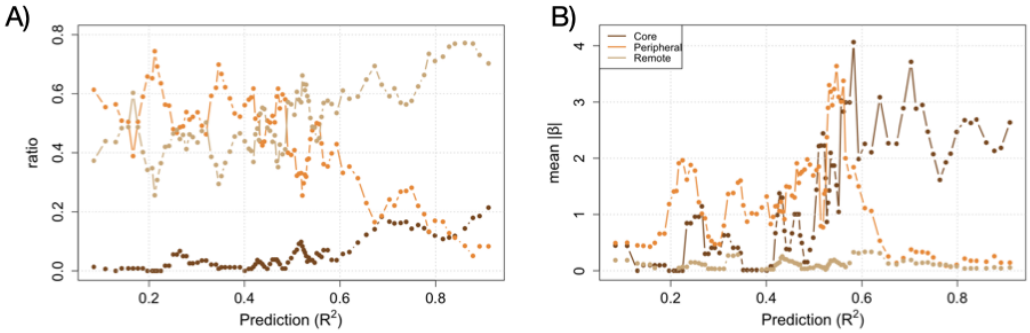

Figure 4. Core, peripheral, and remote determinants of the phenotype. A) Ratio of core, peripheral and remote regulatory connections over the total as function of prediction R^2 for the set of 100 networks (with weight variation sd = 0.1; main text for definition of each connection class). Core determinants (dark brown line) increase with R^2. **B)** Mean of PGS $|\beta|$'s as function of prediction. $|\beta|$'s at intermediate R^2 are dominated by peripheral interactions (orange line). Both plots show rolling windows analysis of the relevant measure sorted by increasing R^2, windows of size 5.

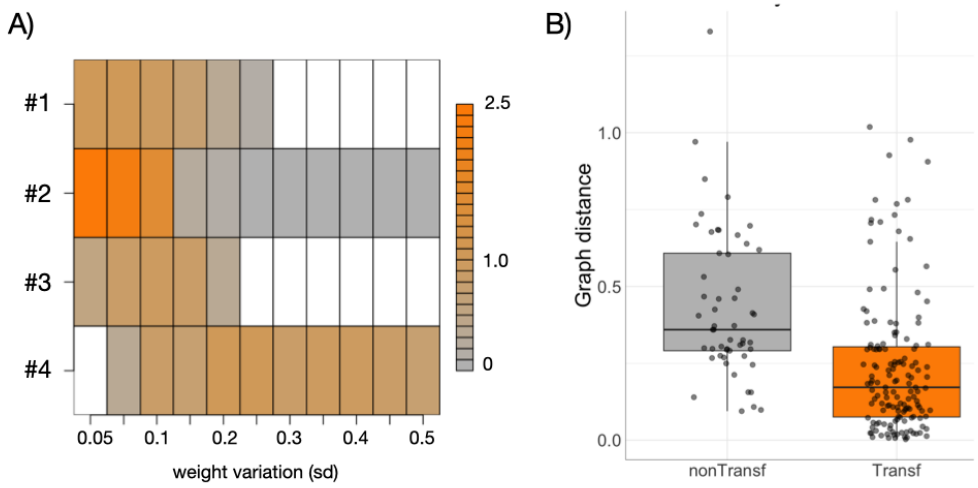

Figure 5. PGS transferability. Transferability of prediction to populations with different genetic variation, A), or network architecture, B). **A)** A PGS computed for each reference network in Figure 3, and a population weight variance of 10% (sd = 0.1), is applied to predict the phenotypes generated for each corresponding network under different population variations (weight variation). Each row is the corresponding R^2 of the prediction normalized by the R^2 of the reference condition (at sd=0.1). White denotes $R^2 < 0$. **B)** A single regulatory connection of the network associated with pattern #1 (Figure 3) is randomly mutated, assigning a new weight with distribution $\sim \mathcal{N}(0, 1)$. The phenotypes generated with the mutant network are also predicted using the PGS computed with the "wild-type" network (with weight variance of sd = 0.1), and an R^2 value is computed. Nontransferable mutants ($R^2 < 0$) exhibit greater dissimilarity than transferable ones based on a spectral network (graph) distance (Wilcoxon rank sum test p-value < 0.001, Methods). Each dot represent a different mutant of a total of two hundred.